Lifetime measurements of excited states in neutron-rich ^{53}Ti: Benchmarking effective shell-model interactions

A. Goldkuhle, A. Blazhev, C. Fransen, A. Dewald, M. Beckers, B. Birkenbach, T. Braunroth, E. Clément, J. Dudouet, J. Eberth, et al.

Lifetime measurements of excited states in neutron-rich ^{53}Ti: benchmarking effective shell-model interactions

A. Goldkuhle,[1,*] A. Blazhev,[1] C. Fransen,[1] A. Dewald,[1] M. Beckers,[1] B. Birkenbach,[1] T. Braunroth,[1] E. Clément,[2] J. Dudouet,[3,4] J. Eberth,[1] H. Hess,[1] B. Jacquot,[2] J. Jolie,[1] Y.-H. Kim,[5] A. Lemasson,[2] S. M. Lenzi,[6,7] H. J. Li,[2] J. Litzinger,[1] C. Michelagnoli,[2,5] C. Müller-Gatermann,[1,8] B. S. Nara Singh,[9,10] R. M. Pérez-Vidal,[11] D. Ralet,[4] P. Reiter,[1] A. Vogt,[1] N. Warr,[1] and K. O. Zell[1]

[1] *Institut für Kernphysik, Universität zu Köln, 50937 Köln, Germany*
[2] *GANIL, CEA/DRF-CNRS/IN2P3, BP 55027, 14076 Caen Cedex 05, France*
[3] *Université Lyon, Université Claude Bernard Lyon 1, CNRS/IN2P3, IP2I Lyon, UMR 5822, F-69622, Villeurbanne, France*
[4] *Centre de Spectrométrie Nucléaire et de Spectrométrie de Masse - CSNSM, CNRS/IN2P3 and Université Paris-Sud, F-91405 Orsay Campus, France*
[5] *Institut Laue-Langevin, BP 156, 38042 Grenoble Cedex 9, France*
[6] *INFN Sezione di Padova, I-35131 Padova, Italy*
[7] *Dipartimento di Fisica e Astronomia dell'Università di Padova, I-35131 Padova, Italy*
[8] *Physics Division, Argonne National Laboratory, 9700 South Cass Avenue, Lemont, Illinois 60439, USA*
[9] *Nuclear Physics Group, Schuster Laboratory, University of Manchester, Manchester, M13 9PL, UK*
[10] *School of Computing Engineering and Physical Sciences, University of the West of Scotland, Paisley, PA1 2BE, UK*
[11] *Instituto de Física Corpuscular, CSIC-Universidad de Valencia, E-46071 Valencia, Spain*

(Dated: December 1, 2020)

Level lifetimes of the yrast $(5/2^-)$ to $13/2^-$ states in the neutron-rich nucleus ^{53}Ti, produced in a multinucleon-transfer reaction, have been measured for the first time. The recoil distance Doppler-shift method was employed and lifetimes of the excited states were extracted by a lineshape analysis aided by GEANT4-based Monte-Carlo simulations. The experiment was performed at the Grand Accélérateur National d'Ions Lourds facility in Caen, France, by using the Advanced Gamma Tracking Array for the γ-ray detection coupled to the large-acceptance variable mode spectrometer for an event-by-event particle identification and the Cologne plunger for deep-inelastic reactions. Reduced transition probabilities, deduced from the lifetimes, give new information on the nuclear structure of ^{53}Ti, and are used to benchmark different shell-model calculations using established interactions in the *fp* shell.

I. INTRODUCTION

The evolution of the shell structure in exotic nuclei such as neutron-rich titanium isotopes ($Z = 22$) is one of the central topics of current experimental and theoretical research in nuclear physics. This attention can be attributed to the physics phenomena arising from a rearrangement of neutron single-particle levels as protons are removed from the $\pi 1f_{7/2}$ orbital. For example, changes in the energy spacings between the orbitals and/or their arrangement can have a significant impact on global nuclear properties such as nuclear shape. Probably the best known example of an unexpected structural change is the "island of inversion" in neutron-rich exotic nuclei at $N = 20$ (see for example Ref. [1] and the references therein). Due to the promotion of neutrons across the $N = 20$ shell closure, deformed rather than spherical ground-state configurations exist in this island. This phenomenon is due to three aspects, namely, the strong interaction between valence protons and the promoted neutrons, interactions between the promoted neutrons themselves and shifts in the energies of the individual particles [1].

Interactions between protons and neutrons also explain the recently observed existence of sub-shell closure at $N = 34$ [2] and at $N = 32$ [3–6], the latter developing in the isotonic chain ^{58}Fe $\rightarrow$ ^{56}Cr$\rightarrow$ ^{54}Ti $\rightarrow$ ^{52}Ca, as the number of protons in the $\pi 1f_{7/2}$ shell decrease and the doubly-magic ^{48}Ca is approached. [3]. Theoretical studies interpret this sub-shell closure as a result of the spin-orbit splitting of the $\nu 2p_{1/2}$ and $\nu 2p_{3/2}$ orbitals and an attenuation of the $\pi 1f_{7/2} - \nu 1f_{5/2}$ monopole interaction. A decreasing number of protons in the $\pi 1f_{7/2}$ orbital, i.e., from Ni to Ca, leads to an uplift of the $\nu 1f_{5/2}$ orbital in energy. In fact, this effect can cause an inversion of the $\nu 1f_{5/2}$ and $\nu 2p_{1/2}$ orbitals [6], forming a gap between the $\nu 2p_{3/2}$ orbital on one side and $\nu 2p_{1/2}$ and $\nu 1f_{5/2}$ orbitals on the other side, and thus giving rise to the $N = 32$ sub-shell closure [3–5].

To verify these findings, lifetimes of excited states are of great importance, since transition probabilities determined from these lifetimes can be used for testing the nuclear structure theories in this region. A recent publication presented new experimental results on ^{52,54}Ti allowing for an investigation of their nuclear structure [7]. The

* Corresponding author: agoldkuhle@ikp.uni-koeln.de

newly determined transition strengths in ^{52}Ti [7] contradict the previous results of Ref. [8] and show an opposite trend to the literature values of $B(E2; J_1^+ \rightarrow (J-2)_1^+)$ as a function of the yrast spin. The new experimental data on ^{52}Ti are now consistent with those of the neighboring nuclei as well as with predictions of shell-model (SM) calculations [7].

Different experimental techniques were used to study nuclei in this region, such as deep-inelastic reactions (^{52,54}Ti [9]), β decay (^{54,55,56}Ti [4]), Coulomb excitation (^{52,54,56}Ti [10]), fusion reactions (^{55}V and ^{55}Ti [11]), knockout reactions (^{56}Cr [12]; ^{52}Ca [5]; ^{54}Ca [6]), and fragmentation reactions (^{50}Ca, ^{56}Ti [13]) and the recently performed multinucleon-transfer reaction [7].

Odd-mass Ti isotopes with $A \leq 51$ have been investigated [14–17], too. The isotopes ^{45,47,49,51}Ti were studied [18] with the deformed configuration mixing shell model and the effective charges and $E2$ transitions were analyzed in fp shell nuclei, especially Ti isotopes with $A = 44 - 50$ [19]. Lifetimes and lifetime limits in ^{49,51}Ti isotopes were also determined using the Doppler-shift attenuation method [15].

As a direct neighbor of ^{54}Ti$_{32}$, the odd-mass nucleus ^{53}Ti is important to have better understanding of the single-particle orbitals at $N = 32$. Information on excited states in the odd-mass nucleus ^{53}Ti was first reported by a prompt γ-ray spectroscopy study, following the β decay [20]. The knowledge of the yrast cascade in ^{53}Ti was extended via the studies performed with the Gammasphere spectrometer, for which ^{48}Ca beam-induced deep-inelastic reactions on thick ^{208}Pb and ^{238}U targets were used. Excitation energies of states with spins up to $I^\pi = 21/2^-$ were determined for the first time [21]. With special focus on the (sub-)shell closure at $N = 32$, the experimental yrast structure was compared with SM calculations using the well-established interactions GXPF1 and GXPF1A and a good agreement between experimental and theoretical results was found [21]. Preliminary results of level lifetimes in ^{53}Ti from this experiment have been already published in Ref. [22]. Here, we report final lifetime results for ^{53}Ti by comparing experimental γ-ray spectra with GEANT4 Monte-Carlo simulated spectra. Reduced transition probabilities are determined from the lifetimes and are compared with the results of SM calculations using different interactions allowing to benchmark the latter.

II. EXPERIMENT

The recoil distance Doppler-shift (RDDS) experiment was performed at the Grand Accélérateur National d'Ions Lourds (GANIL) in Caen, France. The nuclei of interest, in particular $^{46-54}$Ti, were populated via a multinucleon-transfer reaction induced by a ^{238}U beam at an energy of $E(^{238}\text{U}) = 1608.9\,\text{MeV}$ ($= 6.76\,\text{MeV/u}$) impinging on a $\approx 1.5\,\text{mg/cm}^2$ enriched ^{50}Ti target with a $\approx 0.4\,\text{mg/cm}^2$ thick $^{\text{nat}}$Cu layer backing facing the beam to improve the heat dissipation. Details on the experiment are given in Ref. [7]. The experimental setup was composed of three parts, namely, (i) the Advanced Gamma Tracking Array (AGATA) [23, 24] γ-ray spectrometer consisting of 29 36-fold segmented, encapsulated high-purity germanium (HPGe) crystals in 10 cryostats placed at backward angles with respect to the beam direction, (ii) the VAriable MOde high acceptance Spectrometer (VAMOS++) [25–27], and (iii) the compact plunger for deep inelastic reactions [28]. The reaction products were detected and identified with the large acceptance magnetic spectrometer VAMOS++ using a trajectory reconstruction technique. It consisted of Multi-Wire Proportional Counters (MWPC), four Drift Chambers (DC) and a segmented Ionization Chamber (IC). The horizontal and vertical positions (x, y) required for the trajectory reconstruction are measured by the DC. The IC is used for the measurement of the energy loss ΔE and the total energy E. The Time of Flight (TOF) is determined from the signals of the Dual Position-Sensitive Multi-Wire Proportional Counter (DPS-MWPC) and the MWPC, one of which is positioned at the entrance of the spectrometer and the other one at the entry of the focal plane. The VAMOS++ setup permits the measurement of all the parameters needed for the determination of the mass M, the charge state Q, the atomic number Z and the angles θ_{lab} and φ_{lab} with respect to the target position. Both the target and degrader foils were placed at an angle of 45° with respect to the incoming beam which is close to the grazing angle of the multinucleon-transfer reaction. Data were collected at six nominal target-to-degrader distances between 70 µm and 1000 µm for about 1 day per distance, which results in sensitivity to the expected lifetimes. However, during the experiment, beam-induced changes in the target occurred [29], which had such great effects that the distances between the target and degrader could not be determined directly and precisely. Therefore, an in-depth distance determination was necessary first, which was carried out with Monte-Carlo simulations, see Ref. [7].

III. DATA ANALYSIS AND RESULTS

The reaction products were completely identified on an event-by-event basis using VAMOS++. The matrix of the energy loss obtained in the sum of the first three segments of the ionization chamber versus the total energy measured in the sum of all segments was used for the Z identification. The mass A and mass over charge (A/Q) were obtained from the TOF, the total energy and the magnetic rigidity $(B\rho)$. The procedure for the ion identification is described in Ref. [7]. A Doppler-reconstructed γ-ray spectrum is depicted in Fig. 1, which shows the γ-ray yield correlated to ^{53}Ti. A total of nine transitions in ^{53}Ti could be identified, unambiguously after Doppler correction for the degraded component.

The dominant peak at 1237 keV corresponds to the

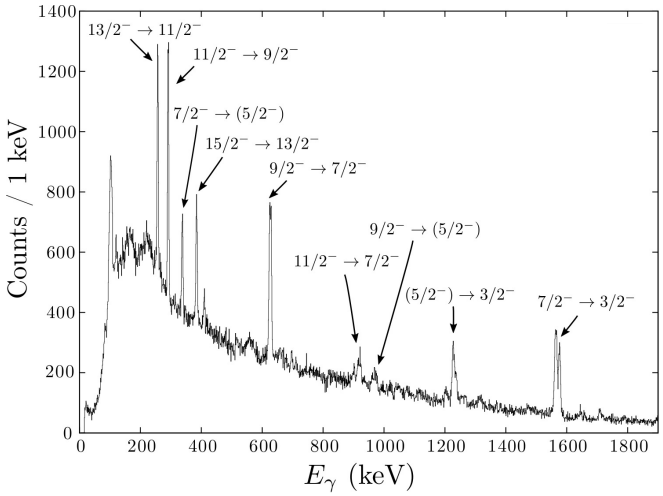

Figure 1. Doppler-corrected γ-ray spectrum in coincidence with ions identified as ^{53}Ti, summed up over all six distances. Nine γ ray decays are observed. Spin-parity assignments taken from Ref. [21]. See text for details.

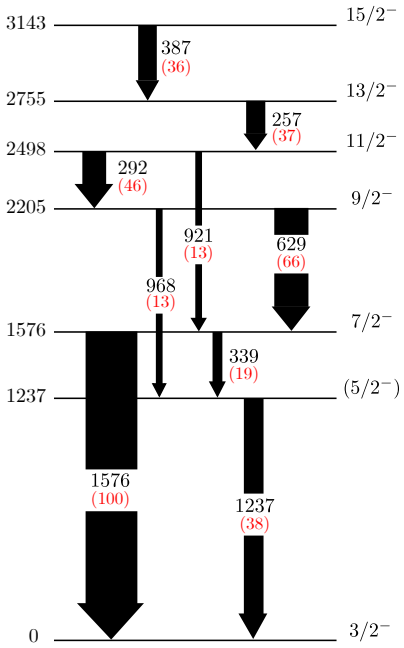

Figure 2. Partial energy level scheme of ^{53}Ti as observed in the present work. All energies are given in keV. Levels with spin-parity assignments taken from Ref. [21]. The thickness of the arrows is proportional to the relative transition intensities (red marked) normalized to the $7/2^- \to 3/2^-$ transition. See text for details.

$(5/2^-) \to 3/2^-_{\text{g.s.}}$ transition. The $(5/2^-)$ state is known to be fed by transitions with 339 keV $(7/2^- \to (5/2^-))$ as well as with 968 keV $(9/2^- \to (5/2^-))$. A further dominant peak can be seen at $E_\gamma = 1576$ keV $(7/2^- \to 3/2^-_{\text{g.s.}})$. The $7/2^-$ state is known to be fed by transitions at 921 keV $(11/2^- \to 7/2^-)$ as well as at 629 keV $(9/2^- \to 7/2^-)$. In addition, three more transitions are visible at $E_\gamma = 292$ keV $(11/2^- \to 9/2^-)$, $E_\gamma = 257$ keV $(13/2^- \to 11/2^-)$ and $E_\gamma = 387$ keV $(15/2^- \to 13/2^-)$. The corresponding level scheme is illustrated in Fig. 2.

Lifetimes of excited states from this data set were determined using the Differential Decay Curve method (DDCM) [30]. Preliminary results of the lifetime analysis revealed slowing-down effects (Doppler Shift Attenuation (DSA)) that was caused by the deceleration of the recoils in the degrader [22]. In Ref. [22], no correction was done to take the effect into account. In the present work, the lifetimes were extracted using Monte-Carlo simulations in order to take the slowing-down effects into account.

The lifetimes are determined by comparing the spectra measured in γ-ray singles and the simulated one obtained by the dedicated Monte-Carlo simulation GEANT4 Toolkit [31]. This tool was developed and has been improved [32] to include the AGATA configuration used in the experiment. An accurate description of the geometry with respect to the foils, beam tube and HPGe detectors provided by the tool, is illustrated in Fig. 3.

Initial values of lifetimes fed to the simulation tool-kit are varied in a range of max. $\tau_{\chi^2_{\text{min}}} \pm 3$ ps in steps of 0.2 ps. For each lifetime assumption, a χ^2 value was calculated following the least-squares method using:

$$\chi^2 = \sum_i \left(\frac{i_{\text{exp}} - i_{\text{sim}}}{\Delta i_{\text{exp}}} \right)^2$$

where i_{exp} (i_{sim}) is the number of counts in bin i in the ex-

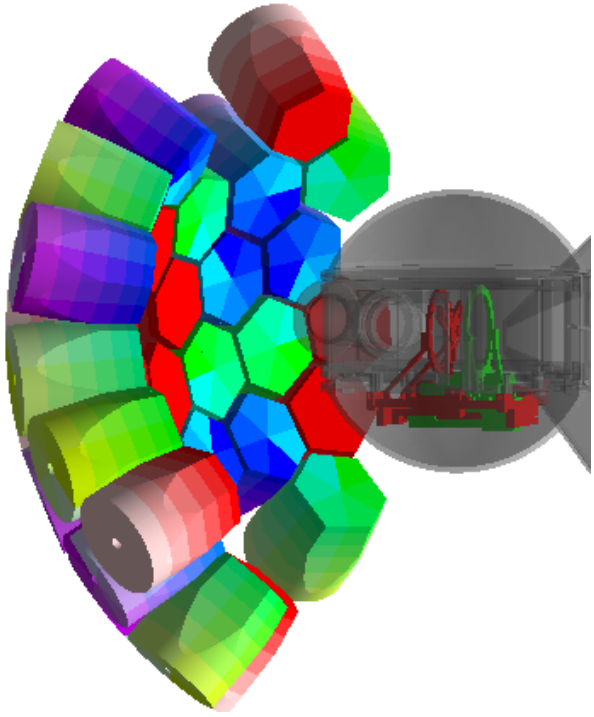

Figure 3. (Color online) Replication of the experimental geometry as provided by the improved GEANT4 toolkit [32]. Shown are the plunger chamber, the detector crystals and their housing. See text for details.

perimental (simulated) spectrum. The simulated statistics are larger than the experimental ones by a factor of 10. The experimental and simulated γ-ray spectra were normalized to each other after a background correction was performed on the simulated spectrum by calculating the background using a ROOT function [33]. The range was chosen to restrict both the fast and slow components of the considered transition. The simulations with the lowest χ^2 value, the experimental spectra and the resulting reduced χ^2 values, which depends on the lifetime value used for the simulation, are presented for five distances in the sensitive range for the $7/2^- \rightarrow 3/2^-_{\text{g.s.}}$ transition in Fig. 4. The lifetime values of the excited states

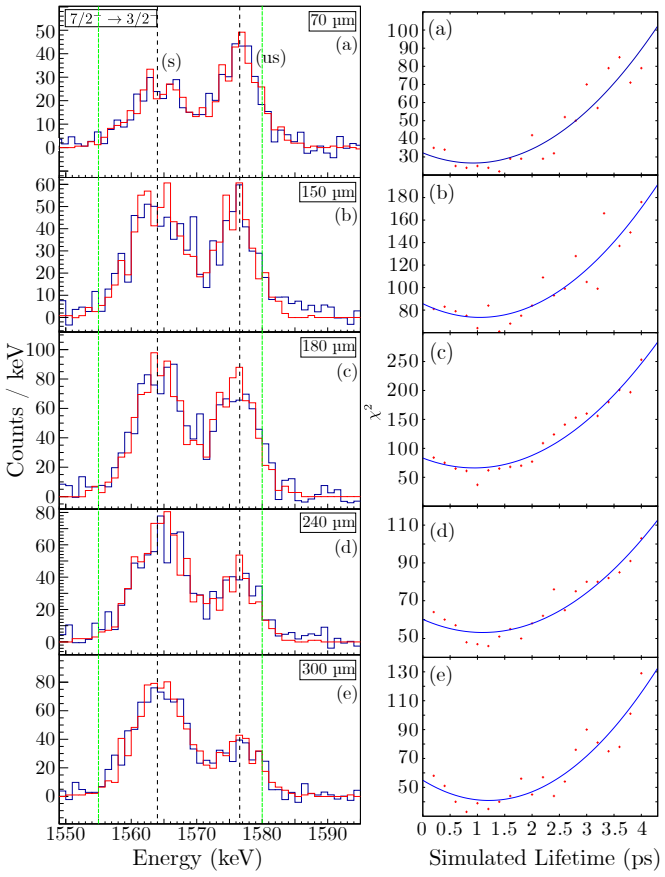

Figure 4. (Color online) Left: Comparison of fits of the simulated GEANT4 γ-ray $7/2^- \rightarrow 3/2^-_{\text{g.s.}}$ transition (red) and measured spectra (blue) at five distances (a-e) used for the lifetime determination. The vertical black dashed lines mark the shifted (s) and unshifted (us) components after Doppler correction for the degraded component, the green dashed lines mark the area used for calculation of the χ^2 values. Right: Reduced χ^2 values (red dots) versus simulated lifetime with a best fitting of the quadratic function (blue line) for each distance. See text for details.

of interest were fixed from top to bottom in the level scheme with respect to the excitation energies. The population ratios of the individual states were determined from the γ-ray spectrum summed over all distances and were utilized to perform simulations. The final lifetime results from the average of the individual lifetime values of each target-to-degrader distance. The statistical error of the lifetime determined by the χ^2 method is derived from the lifetimes with $\chi^2 + 1$.

The final results for lifetimes of the $(5/2^-)$ to $13/2^-$ states in ^{53}Ti are summarized in Table I. For the $15/2^-$ state, an effective lifetime with $\tau = 2.2$ ps was assumed, because the separation of the shifted and degraded components was not possible. In addition, the low statistics of this transition (to the $13/2^-$ state) made the determination of the actual lifetime of the $15/2^-$ state impossible. This effective lifetime is the cumulative lifetime of the $15/2^-$ state including all feeding times of all of the higher-lying levels, including those that were not observed. With the exception of the $9/2^-$ state, the lifetimes determined in this work are consistent with the lifetime values within the error limits determined using DDCM in Ref. [22]. It should be highlighted that the lifetime value of the $9/2^-$ state differs from the previous value [22] because the determination in the present work has been done by taking the slowing-down effects in to account.

Table I. Results of the lifetime analysis ^{53}Ti by means of simulations. See text for details.

$J_i \rightarrow J_f$	E_γ^{lit} [21] (keV)	$\tau_{\text{present}}(J_i)$ (ps)
$(5/2^-) \rightarrow 3/2^-_{\text{g.s.}}$	1237.1	1.5(9)
$7/2^- \rightarrow 3/2^-_{\text{g.s.}}$	1576.3	1.0(4)
$9/2^- \rightarrow (5/2^-)$	968.6	2.8(7)
$11/2^- \rightarrow 7/2^-$	921.8	3.2(5)
$13/2^- \rightarrow 11/2^-$	257.8	2.9(5)

IV. DISCUSSION

The nuclear shell model has proved to be rather successful in describing experimental excitation energies of even-even neutron-rich titanium and neighboring nuclei [4, 6, 9, 10]. On the other hand, although the order of magnitude of $E2$ strengths for the even-even Ti isotopes above $N = 28$ could be reproduced, the experimental values showed some pronounced staggering for the lowest transition, which could not be accounted for by the theory [8, 10]. Our recent experimental results on ^{52,54}Ti [7] and especially the considerable revision of the $E2$ strength from the 2_1^+ and 4_1^+ states in ^{52}Ti, greatly reduced the above-mentioned $B(E2; 2_1^+ \rightarrow 0^+_{\text{g.s.}})$ staggering and with respect to the $E2$ strengths of the yrast band in ^{52}Ti solved previous contradiction with theory.

In the neighboring ^{53}Ti, the yrast nuclear structure was discussed by Fornal *et al.* [21] in the light of SM calculations using the FPD6 [34] and GXPF1(A) [35] interactions, although without having information on experimental transition strengths. In this section, based on

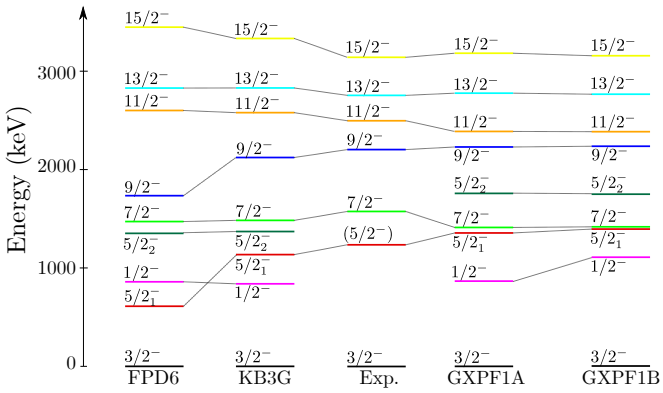

Figure 5. (Color online) Comparison of experimental level energies for ^{53}Ti and the results of the full fp shell-model calculations using the FPD6, GXPF1A, GXPF1B, and KB3G interactions. See text for details.

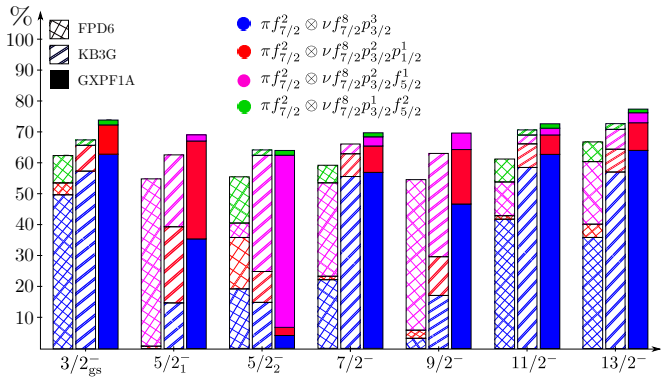

Figure 6. (Color online) Leading neutron configurations of selected states up to $13/2^-$ with corresponding proton configuration $\pi f^2_{7/2}$. Configurations with contributions >5% for at least one interaction are shown. See text for details.

our new experimental results, we address again the nuclear structure of ^{53}Ti comparing with SM calculations in the fp model space. These calculations were performed with the NuShellX@MSU code [36] using four established effective interactions, namely, FPD6 [34], KB3G [37], GXPF1A [35] and GXPF1B [38]. For all interactions, effective charges of $e_\pi = 1.31\,e$ and $e_\nu = 0.46\,e$ [39] were used to calculate $B(E2)$ values, which proved to be a good choice in our previous publication [7]. All $M1$ strengths were calculated using free-nucleon g factors $g^s_p = 5.586$, $g^s_n = -3.826$, $g^l_p = 1.0$, and $g^l_n = 0.0$ as the spin-orbit partner orbitals are all present in the model space as well as to ease the comparison between the theories.

In Fig. 5, a partial level scheme of ^{53}Ti is compared to SM calculations using the above-mentioned interactions. With the exception of the FPD6 interaction, the calculated energies agree well with the experimental ones. An almost perfect match is provided by the KB3G interaction, which, in contrast to the GXPF1A and GXPF1B interactions, has a clear separation of the $5/2^-_1$ and $7/2^-$ levels, similar in magnitude to the experiment. The FPD6 interaction predicts lower energies for the $5/2^-_1$ and $9/2^-$ states leading to an inversion of the $1/2^-$ and $5/2^-_1$ states and a considerable splitting between $5/2^-_1$ and $7/2^-$, as well as $9/2^-$ and $11/2^-$, which contradicts the experiment. This is due to known "monopole defects" of the FPD6, which, above $N = 28$, result in a lower position of the $\nu f_{5/2}$ orbital and a higher position of $\nu p_{1/2}$, and has been discussed already in Ref. [37]. The shift of the $1/2^-$ state from GXPF1A to GXPF1B observed in Fig. 5 results from an increase in the single-particle energy of the $\nu p_{1/2}$ orbital and a modification of the matrix elements involving this orbital [38]. Since the $1/2^-$ state is still experimentally unknown it will not be discussed here. Figure 6 contains the leading wave function configurations of the valence neutrons of selected states in ^{53}Ti resulting from SM calculations with FPD6, KB3G and GXPF1A. For all cases shown, the corresponding proton configuration is $\pi f^2_{7/2}$, which is by far the most dominant one. As the numbers for GXPF1A and GXPF1B for the discussed states are very similar, both for the wave functions and consequently for the transition strengths, in the following, only the GXPF1A results are shown and discussed.

As shown in Fig. 6 and already discussed by Fornal *et al.* [21], the GXPF1A interaction predicts that the structure of the yrast states with spins from $I = 3/2$ to $13/2$ is dominated at the level of 35-65% by a single SM configuration $\pi f^2_{7/2} \otimes \nu f^8_{7/2} p^3_{3/2}$ (depicted in blue), which corresponds to one neutron hole in the $p_{3/2}$ orbital, i.e. in the $N = 32$ subshell closure. The second most dominant neutron configuration according to GXPF1A is the $\nu f^8_{7/2} p^2_{3/2} p^1_{1/2}$ (depicted in red) and is particularly strong for the $5/2^-_1$ and $9/2^-$ states. The predictions using the KB3G interaction for the structures of the $3/2^-, 7/2^-, 11/2^-, 13/2^-$ states is similar to that of GXPF1A. In the case of the $5/2^-$ and $9/2^-$ states apart from blue and red configurations, KB3G predicts significant mixing also from $\nu f^8_{7/2} p^2_{3/2} f^1_{5/2}$ configuration (depicted in pink). In particular the pink configuration dominates for the $9/2^-$ state. The leading configurations of the FPD6 clearly distinguish themselves from the other two interactions. As mentioned, due to the low-lying $\nu f_{5/2}$ orbital, the discussed yrast states have strong or dominant configurations in which one or more neutrons occupy that orbital (see Fig. 6). This is especially obvious for the $5/2^-_1$ state and will be discussed later in the discussion.

Although the energies of the excited states can differentiate between the SM interactions, a better benchmarking of the latter can be done by experimental reduced transition probabilities. This work presents the first experimental results on state lifetimes in ^{53}Ti from which data of reduced strengths have been obtained and compared with the calculated values.

The results of the theoretical and experimental electric and magnetic transition strengths are given in Fig. 7,

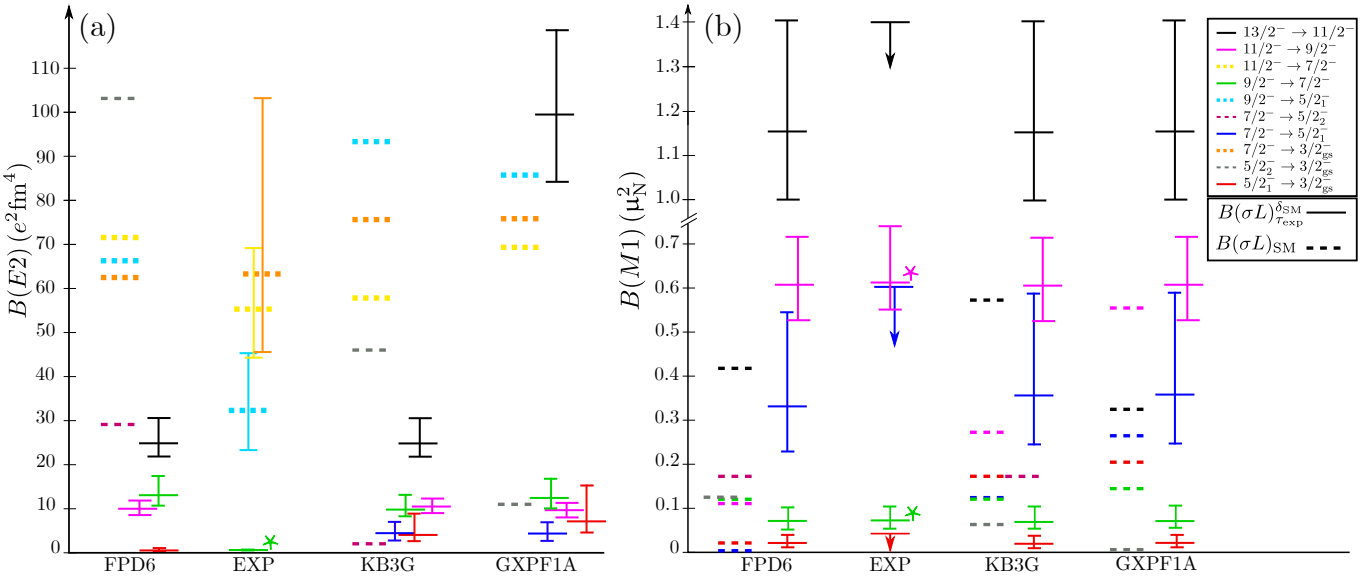

Figure 7. (Color online) Comparison of experimental $B(M1)_{\mathrm{exp}}$, $B(E2)_{\mathrm{exp}}$ values and results $B(\sigma L)_{\mathrm{SM}}$ (dashed lines) of the full *fp* shell-model calculations using the FPD6, GXPF1A, and KB3G interactions for transitions of mixed $E2/M1$ and pure $E2$ character in ^{53}Ti. For transitions where experimental $E2/M1$ multipole mixing ratios are available [21], the transition strengths are marked with an $*$, while for the other mixed transitions upper limits of the transition strengths were calculated by assuming the extreme cases of pure $E2$ transitions. $B(\sigma L)^{\delta_{\mathrm{SM}}}_{\tau_{\mathrm{exp}}}$ (solid lines) contains transition strengths, calculated from the experimental lifetimes using mixing ratios deduced from the respective shell-model $E2$ and $M1$ strength and the corresponding E_γ^{exp}. See text for details and Table II in the Appendix for the numerical values.

whose numerical values are listed in Table II in the Appendix. The transitions $13/2^- \to 11/2^-$, $11/2^- \to 9/2^-$, $9/2^- \to 7/2^-$, $7/2^- \to (5/2^-)$ and $(5/2^-) \to 3/2^-$ are of mixed $E2/M1$ multipolarity and therefore one needs to know the multipole mixing ratio $\delta(E2/M1)$, defined as the ratio of the corresponding transition probabilities [40]. A pure $M1$ transition would have a value of $\delta(E2/M1)$ equal to zero, while an infinite value corresponds to a pure $E2$ transition. The knowledge of $\delta(E2/M1)$ for the above transitions is limited. In Ref. [21] values of $\arctan(\delta)$ are given for $9/2^- \to 7/2^-$ and $11/2^- \to 9/2^-$, from which we calculate $(9/2^- \to 7/2^-)$ $|\delta(E2/M1)| = 0.0133 \pm 0.0003$ and $(11/2^- \to 9/2^-)$ $|\delta(E2/M1)| = 0.052 \pm 0.018$, testifying a dominant $M1$ character and allowing to extract the $B(E2)_{\mathrm{exp}}$ and $B(M1)_{\mathrm{exp}}$ (marked with an $*$ in the figure). Due to the scaling of Fig. 7 (a), the $B(E2; 11/2^- \to 9/2^-)_{\mathrm{exp}} = 280^{+230}_{-160}\, e^2\mathrm{fm}^4$ is not shown. For the other transitions of mixed $E2/M1$ character, upper limits of $B(E2)_{\mathrm{exp}}$ and $B(M1)_{\mathrm{exp}}$ were calculated assuming the extreme cases of a pure $E2$ or a pure $M1$ character. The error bars (upper limits) of the $B(\sigma L)_{\mathrm{exp}}$ and $B(\sigma L)^{\delta_{\mathrm{SM}}}_{\tau_{\mathrm{exp}}}$ (solid lines) are determined largely by the error bars of the state lifetimes and branching ratios, as well as, to a minor degree, by the error bars of the above δ_{exp}, where applicable.

With respect to the $\Delta J = 2$ $E2$ transitions, all theoretical results have a good agreement with the experimental values for the $7/2^- \to 3/2^-_{\mathrm{g.s.}}$ and $11/2^- \to 7/2^-$ transitions within the error bars, while the $9/2^- \to (5/2^-)$ transition strength is overestimated by all presented calculations (see Fig. 7 (a)). For the mixed $E2/M1$ transitions, obviously the upper limits of $B(E2)_{\mathrm{exp}}$ (not shown in Fig. 7) are much larger than the SM $E2$ strengths, and their magnitude shows that these transitions must have a dominant $M1$ character. This is nicely reproduced by the theory, which also predicts dominant $M1$ components. Using the SM $E2$ and $M1$ matrix elements of the corresponding interaction and the E_γ^{exp}, we calculate SM-based multipole mixing ratios (see Table II in the Appendix). Then, using these δ_{SM} and the experimental lifetimes, we calculate $B(M1)^{\delta_{\mathrm{SM}}}_{\tau_{\mathrm{exp}}}$ and $B(E2)^{\delta_{\mathrm{SM}}}_{\tau_{\mathrm{exp}}}$ (solid lines), which should present a more realistic estimate of "experimental" strengths than the upper limits of pure $E2$ or $M1$ strengths. Since the $E2$ strengths for mixed transitions ($\Delta J = 1$) are highly sensitive to the value of $\delta(E2/M1)$, only the more precise and extremely low $B(E2; 9/2^- \to 7/2^-)$ value could be meaningfully compared with the calculations, of which all fail to reproduce it. On the other hand, the $M1$ components are not so sensitive to the $\delta(E2/M1)$, and the resulting $B(M1)_{\mathrm{exp}}$ as well as $B(M1)^{\delta_{\mathrm{SM}}}_{\tau_{\mathrm{exp}}}$ values, could be used to test the SM interactions (see Fig. 7 (b)). When comparing the experimental and SM $B(M1)$ values presented in Fig 7 (b), one notices several points. The $B(M1)_{\mathrm{exp}}$ strength of the $9/2^- \to 7/2^-$ transition is well reproduced by all interactions.

The $B(M1; 11/2^- \to 9/2^-)_{\mathrm{exp}}$ value is reproduced only by the GXPF1A interaction. Generally, the SM $M1$ strengths agree with the experimental upper limits for the $7/2^- \to (5/2^-)$ and $13/2^- \to 11/2^-$ transitions,

but only GXPF1A matches the $B(M1)^{\delta_{\rm SM}}_{\tau_{\rm exp}}$ value for the $7/2^- \rightarrow 5/2^-_1$, while all of the other interactions underestimate the large $B(M1; 13/2^- \rightarrow 11/2^-)^{\delta_{\rm SM}}_{\tau_{\rm exp}}$ value by factor of 2 to 3.

The most interesting case for us presents the $M1$ strength of the $(5/2^-) \rightarrow 3/2^-$ transition. While both improved interactions, KB3G and GXPF1A, overestimate the $B(M1; (5/2^-) \rightarrow 3/2^-)_{\rm exp}$ limit by about a factor of 4 to 5, only the deficient FPD6 reproduces the experimental limit and the $B(M1)^{\delta_{\rm SM}}_{\tau_{\rm exp}}$ estimate correctly. An inspection of the leading neutron configurations for the relevant states (see Fig. 6) shows that the difference is found in the predicted nuclear structure of the $5/2^-_1$ state. While the FPD6 predicts a dominant neutron configuration $\nu f^8_{7/2} p^2_{3/2} f^1_{5/2}$ ($\sim 55\,\%$) with the protons coupled to spin zero, in GXPF1A the dominant configuration is $\nu f^8_{7/2} p^3_{3/2}$ ($\sim 36\,\%$) with the protons are coupled to spin 2, as well as about 32 % of $\nu f^8_{7/2} p^2_{3/2} p^1_{1/2}$. Although the calculations using the KB3G interaction predict a more mixed wave function made out of three leading neutron configurations, the main similarity to the calculations performed with the GXPF1A interaction and main difference to those using the FPD6 interaction is the considerable amount of ($\sim 25\,\%$) $\nu f^8_{7/2} p^2_{3/2} p^1_{1/2}$ configuration. Thus, the relatively strong $B(M1; 5/2^-_1 \rightarrow 3/2^-)$ in KB3G and GXPF1A can be explained by spin-flip transitions $\nu p_{1/2} \leftrightarrow \nu p_{3/2}$. In contrast, the small $B(M1)$ value predicted by the FPD6 interaction corresponds to the strong decrease of spin-flip components $\nu p_{1/2} \leftrightarrow \nu p_{3/2}$. As Fig. 5 shows, the FPD6 energy of the $5/2^-_1$ is significantly lower than that from the experiment value, while the $5/2^-_2$ state is close to the experimental $(5/2^-)$ state. In order to compare the properties of the $5/2^-_2$ states in the different interactions, we have shown their theoretical energies in Fig. 5, their configurations in Fig. 6 and results for two transitions in Fig. 7. Figure 6 reveals that the neutron configurations of the calculated $5/2^-_2$ states are more mixed, but the common feature for all interactions is that when compared to the corresponding $5/2^-_1$ state, there is an exchange of the dominant configurations with respect to the orbital where the odd neutron resides. To give an example, in FPD6 the $\nu f^8_{7/2} p^2_{3/2} f^1_{5/2}$ configuration is dominant in $5/2^-_1$, but one of the least in $5/2^-_2$. This yields a clearly changed amount of $\nu p_{1/2} \leftrightarrow \nu p_{3/2}$ strength for the $5/2^-_2 \rightarrow 3/2^-$ $M1$ transition which is shown in Fig. 7 (b). For each of the interactions, one can see the direct relation between the percentage of $\nu f^8_{7/2} p^2_{3/2} p^1_{1/2}$ in the wave functions of the $5/2^-_{1,2}$ states and their $M1$ strength to the ground state. Thus, apparently the "proper" amount of $\nu p^1_{1/2}$ component in the wave function of the $5/2^-_1$ state seems to be crucial in describing the $B(M1; 5/2^-_1 \rightarrow 3/2^-)$ strength.

In addition to this main component, other $M1$ strengths could come from spin-flip transitions of the type $f_{7/2} \leftrightarrow f_{5/2}$. The amount of proton $f_{7/2} \leftrightarrow f_{5/2}$ components should be nearly independent of the neutron single-particle energies and proton-truncated calculations showed minimal effect on these SM $B(M1)$ strengths. Therefore, we have studied the effect of neutron excitations from the $f_{7/2}$ orbital across the $N = 28$ shell to the calculated $B(M1; 5/2^-_1 \rightarrow 3/2^-)$ strength. In the case of FPD6, these effects work constructively and double the strength from $0.01\,\mu^2_N$, in the truncated calculation, to the $0.02\,\mu^2_N$ in the non-truncated one. On the other hand in KB3G and GXPF1A, the configurations with $np-nh$ neutron excitations across the $N = 28$ shell work destructively, reducing the amount of $\nu p^3_{3/2}$ configuration in the $3/2^-_{\rm g.s.}$ state and of the $\nu p^2_{3/2} p^1_{1/2}$ configuration in the $5/2^-_1$ state, thus leading to a reduction of the $M1$ strengths down to the values shown in Fig. 7 (b).

Altogether, we come to the conclusion, that the $B(M1; 5/2^-_1 \rightarrow 3/2^-)$, as well as other $M1$ strengths in ^{53}Ti, play a special role in benchmarking and understanding the nuclear structure in this and neighboring nuclei. At the moment, none of the presented effective SM Hamiltonians could describe simultaneously all of the newly measured transition strengths. Therefore, it would be interesting to see how interactions including three-body forces [41] and, in particular, the microscopic $NN + 3N$ interaction [42] in the extended $pfg_{9/2}$ model space would perform for ^{53}Ti. Recently, this interaction was successfully used to describe the magnetic moment of the $3/2^-_{\rm g.s.}$ in ^{51}Ca [43], which is the $N = 31$ isotone of ^{53}Ti. One should mention that this $NN + 3N$ interaction also predicts a "low-lying" $5/2^-_1$ state in ^{49}Ca, but nevertheless it describes the excited spectrum of ^{51}Ca similarly as well as KB3G, and better than GXPF1A (see Fig. 10 of Ref. [42]), which indicates that this interaction may well solve the issue of the $\nu p_{1/2}$ occupation and the $B(M1; 5/2^-_1 \rightarrow 3/2^-)$ strength in ^{53}Ti.

V. SUMMARY

In this work, the $5/2^-$ to $15/2^-$ states of the yrast band in ^{53}Ti were populated in a multinucleon-transfer reaction and their lifetimes were measured with the recoil distance Doppler-shift technique for the first time. The analysis required a precise preparation of the data, followed by the extraction of lifetimes of the excited states by comparing the γ-ray line shapes from GEANT4 Monte-Carlo simulations with experimental Doppler-corrected transitions and a χ^2 minimization. Both the level scheme and the electric and magnetic transition probabilities were compared to predictions of shell-model calculations using the established fp interactions KB3G, GXPF1A, GXPF1B, and FPD6. The level scheme can be described best with KB3G, but also calculations with GXPF1A and GXPF1B perform fairly well. The transition probabilities are not reproduced simultaneously by any of the presented theoretical calculations. A special attention is drawn to the $B(M1; 5/2^-_1 \rightarrow 3/2^-)$ value which is determined to be relatively low, in contradiction to the predic-

tions of the established KB3G, GXPF1A and GXPF1B interactions. An important aspect of that $M1$ strength is the amount of $\nu p^1_{1/2}$ components in the wave function of the yrast $(5/2^-)$ state. Further developments on the theory side are required in order to explain these transition strengths. Improved experimental information would be also beneficial. For example, due to missing $E2/M1$ mixing ratios, absolute transition probabilities for $\Delta J = 1$ transitions cannot be used for a further test of the performed SM calculations. Of similar importance is also the experimental identification of the $1/2^-_1$ state.

ACKNOWLEDGMENTS

The authors are grateful to the GANIL staff for the professional support during the experiment. The research leading to these results has received from the German BMBF under contract No. 05P18PKFN9 and No. 05P19PKFNA, the European Union Seventh Framework through ENSAR under contract No. 262010 and partially supported by Ministry of Science, Spain, under the grants FPA2017-84756-C4 and SEV-2014-0398, by the EU FEDER funds, and by the U.S. Department of Energy, Office of Science, Office of Nuclear Physics, under contract No. DE-AC02-06CH11357.

[1] E. K. Warburton, J. A. Becker, and B. A. Brown, Mass systematics for $A = 29-44$ nuclei: The deformed $A \sim 32$ region, Phys. Rev. C **41**, 1147 (1990).
[2] S. Chen, J. Lee, P. Doornenbal, A. Obertelli, C. Barbieri, Y. Chazono, P. Navrátil, K. Ogata, T. Otsuka, F. Raimondi, et al., Quasifree neutron knockout from ^{54}Ca corroborates arising $n = 34$ neutron magic number, Phys. Rev. Lett. **123**, 142501 (2019).
[3] J. Prisciandaro, P. Mantica, B. Brown, D. Anthony, M. Cooper, A. Garcia, D. Groh, A. Komives, W. Kumarasiri, P. Lofy, et al., New evidence for a subshell gap at $N = 32$, Physics Letters B **510**, 17 (2001).
[4] S. N. Liddick, P. F. Mantica, R. Broda, B. A. Brown, M. P. Carpenter, A. D. Davies, B. Fornal, T. Glasmacher, D. E. Groh, M. Honma, et al., Development of shell closures at $N = 32, 34$. I. β decay of neutron-rich Sc isotopes, Phys. Rev. C **70**, 064303 (2004).
[5] A. Gade, R. V. F. Janssens, D. Bazin, R. Broda, B. A. Brown, C. M. Campbell, M. P. Carpenter, J. M. Cook, A. N. Deacon, D.-C. Dinca, et al., Cross-shell excitation in two-proton knockout: Structure of ^{52}Ca, Phys. Rev. C **74**, 021302 (2006).
[6] D. Steppenbeck, S. Takeuchi, N. Aoi, P. Doornenbal, M. Matsushita, H. Wang, H. Baba, N. Fukuda, S. Go, M. Honma, et al., Evidence for a new nuclear 'magic number' from the level structure of ^{54}Ca, Nature **502**, 207 (2013).
[7] A. Goldkuhle, C. Fransen, A. Blazhev, M. Beckers, B. Birkenbach, T. Braunroth, E. Clément, A. Dewald, J. Dudouet, J. Eberth, et al. (AGATA Collaboration), Lifetime measurements in ^{52,54}Ti to study shell evolution toward $N = 32$, Phys. Rev. C **100**, 054317 (2019).
[8] K.-H. Speidel, J. Leske, S. Schielke, S. Bedi, O. Zell, P. Maier-Komor, S. Robinson, Y. Sharon, and L. Zamick, Low-level structure of ^{52}Ti based on g factor and lifetime measurements, Physics Letters B **633**, 219 (2006).
[9] R. Janssens, B. Fornal, P. Mantica, B. Brown, R. Broda, P. Bhattacharyya, M. Carpenter, M. Cinausero, P. Daly, A. Davies, et al., Structure of ^{52,54}Ti and shell closures in neutron-rich nuclei above 48Ca, Physics Letters B **546**, 55 (2002).
[10] D.-C. Dinca, R. V. F. Janssens, A. Gade, D. Bazin, R. Broda, B. A. Brown, C. M. Campbell, M. P. Carpenter, P. Chowdhury, J. M. Cook, et al., Reduced transition probabilities to the first 2^+ state in ^{52,54,56}Ti and development of shell closures at $N = 32, 34$, Phys. Rev. C **71**, 041302 (2005).
[11] S. Zhu, R. Janssens, B. Fornal, S. Freeman, M. Honma, R. Broda, M. Carpenter, A. Deacon, B. Kay, F. Kondev, et al., One-particle excitations outside the ^{54}Ti semi-magic core: The ^{55}V and ^{55}Ti yrast structures, Physics Letters B **650**, 135 (2007).
[12] A. Gade, R. V. F. Janssens, D. Bazin, B. A. Brown, C. M. Campbell, M. P. Carpenter, J. M. Cook, A. N. Deacon, D.-C. Dinca, S. J. Freeman, et al., One-neutron knockout in the vicinity of the $N = 32$ sub-shell closure: ^{9}Be(^{57}Cr,^{56}Cr+γ)X, Phys. Rev. C **74**, 047302 (2006).
[13] P. Maierbeck, *Untersuchung von Ein-Teilchen-Zuständen in neutronenreichen Kalzium- und Titanisotopen*, Dissertation, Technische Universität München.
[14] M. Niikura, E. Ideguchi, N. Aoi, H. Baba, T. Fukuchi, Y. Ichikawa, H. Iwasaki, T. Kubo, M. Kurokawa, M. Liu, et al., Yrast spectroscopy in $^{49-51}$Ti via fusion-evaporation reaction induced by a radioactive beam, The European Physical Journal A **42**, 471 (2009).
[15] N. Taccetti, P. A. Mando, P. Sona, and K. P. Lieb, Lifetime measurements in ^{49}Ca and ^{51}Ti, Journal of Physics G: Nuclear Physics **13**, 393 (1987).
[16] P. A. Mandò, G. Poggi, P. Sona, and N. Taccetti, γ decay and lifetimes of excited levels in ^{49}Ti, Phys. Rev. C **23**, 2008 (1981).
[17] J. Weaver, M. Grace, D. Start, R. Zurmühle, D. Balamuth, and J. Noé, Lifetime and angular-correlation measurements in ^{47}Ti, Nuclear Physics A **196**, 269 (1972).
[18] A. Dhar, D. Kulkarni, and K. Bhatt, The energy spectra and electromagnetic transitions of odd-a titanium isotopes, Nuclear Physics A **285**, 93 (1977).
[19] A. K. Dhar and K. H. Bhatt, Effective charges and $E2$ transitions in $1f-2p$ shell nuclei, Phys. Rev. C **16**, 792 (1977).

[20] L. A. Parks, C. N. Davids, and R. C. Pardo, β decay and mass of the new neutron-rich isotope ^{53}Ti, Phys. Rev. C **15**, 730 (1977).

[21] B. Fornal, S. Zhu, R. V. F. Janssens, M. Honma, R. Broda, B. A. Brown, M. P. Carpenter, S. J. Freeman, N. Hammond, F. G. Kondev, et al., Yrast structure of neutron-rich ^{53}Ti, Phys. Rev. C **72**, 044315 (2005).

[22] A. Goldkuhle, C. Fransen, A. Dewald, N. Alahari, M. Beckers, B. Birkenbach, A. Blazhev, T. Braunroth, E. Clément, G. De France, et al., Preliminary results of lifetime measurements in neutron-rich ^{53}Ti, EPJ Web Conf. **223**, 01022 (2019).

[23] S. Akkoyun, A. Algora, B. Alikhani, F. Ameil, G. de Angelis, L. Arnold, A. Astier, A. Ataç, Y. Aubert, C. Aufranc, et al., AGATA-Advanced GAmma Tracking Array, Nuclear Instruments and Methods in Physics Research Section A: Accelerators, Spectrometers, Detectors and Associated Equipment **668**, 26 (2012).

[24] E. Clément, C. Michelagnoli, G. de France, H. Li, A. Lemasson, C. B. Dejean, M. Beuzard, P. Bougault, J. Cacitti, J.-L. Foucher, et al., Conceptual design of the AGATA 1π array at GANIL, Nuclear Instruments and Methods in Physics Research Section A: Accelerators, Spectrometers, Detectors and Associated Equipment **855**, 1 (2017).

[25] S. Pullanhiotan, M. Rejmund, A. Navin, W. Mittig, and S. Bhattacharyya, Performance of VAMOS for reactions near the Coulomb barrier, Nuclear Instruments and Methods in Physics Research Section A: Accelerators, Spectrometers, Detectors and Associated Equipment **593**, 343 (2008).

[26] M. Rejmund, B. Lecornu, A. Navin, C. Schmitt, S. Damoy, O. Delaune, J. Enguerrand, G. Fremont, P. Gangnant, L. Gaudefroy, et al., Performance of the improved larger acceptance spectrometer: VAMOS++, Nuclear Instruments and Methods in Physics Research Section A: Accelerators, Spectrometers, Detectors and Associated Equipment **646**, 184 (2011).

[27] M. Vandebrouck, A. Lemasson, M. Rejmund, G. Frémont, J. Pancin, A. Navin, C. Michelagnoli, J. Goupil, C. Spitaels, and B. Jacquot, Dual Position Sensitive MWPC for tracking reaction products at VAMOS++, Nuclear Instruments and Methods in Physics Research Section A: Accelerators, Spectrometers, Detectors and Associated Equipment **812**, 112 (2016).

[28] A. Dewald, O. Möller, and P. Petkov, Developing the Recoil Distance Doppler-Shift technique towards a versatile tool for lifetime measurements of excited nuclear states, Progress in Particle and Nuclear Physics **67**, 786 (2012).

[29] Ch. Stodel, M. Toulemonde, C. Fransen, B. Jacquot, E. Clément, G. Frémont, M. Michel, and C. Dufour, "Thermal Spike" model applied to thin targets irradiated with swift heavy ion beams at few MeV/u, EPJ Web Conf. **229**, 05001 (2020).

[30] A. Dewald, S. Harissopulos, and P. von Brentano, The differential plunger and the differential decay curve method for the analysis of recoil distance Doppler-shift data, Zeitschrift für Physik A Atomic Nuclei **334**, 163 (1989).

[31] S. Agostinelli, J. A. K. Amako, J. Apostolakis, H. Araujo, P. Arce, M. Asai, D. Axen, S. Banerjee, G. Barrand, F. Behner, et al., Geant4-a simulation toolkit, Nuclear Instruments and Methods in Physics Research Section A: Accelerators, Spectrometers, Detectors and Associated Equipment **506**, 250 (2003).

[32] T. Braunroth, private communication (2019).

[33] R. Brun and F. Rademakers, ROOT – An object oriented data analysis framework, Nuclear Instruments and Methods in Physics Research Section A: Accelerators, Spectrometers, Detectors and Associated Equipment **389**, 81 (1997), new Computing Techniques in Physics Research V.

[34] W. Richter, M. V. D. Merwe, R. Julies, and B. Brown, New effective interactions for the 0f1p shell, Nuclear Physics A **523**, 325 (1991).

[35] M. Honma, T. Otsuka, B. A. Brown, and T. Mizusaki, Shell-model description of neutron-rich pf-shell nuclei with a new effective interaction GXPF1, The European Physical Journal A - Hadrons and Nuclei **25**, 499 (2005).

[36] B. Brown and W. Rae, The Shell-Model Code NuShellX@MSU, Nuclear Data Sheets **120**, 115 (2014).

[37] A. Poves, J. Sánchez-Solano, E. Caurier, and F. Nowacki, Shell model study of the isobaric chains $A = 50$, $A = 51$ and $A = 52$, Nuclear Physics A **694**, 157 (2001).

[38] M. Honma, T. Otsuka, and T. Mizusaki, Shell-model description of neutron-rich Ca isotopes, RIKEN Accel. Prog. Rep. **41**, 32 (2008).

[39] M. Dufour and A. P. Zuker, Realistic collective nuclear Hamiltonian, Phys. Rev. C **54**, 1641 (1996).

[40] J. M. Blatt, V.F. Weisskopf, *Theoretical Nuclear Physics* (Springer-Verlag, New York, 1979).

[41] H.-W. Hammer, A. Nogga, and A. Schwenk, Colloquium: Three-body forces: From cold atoms to nuclei, Rev. Mod. Phys. **85**, 197 (2013).

[42] J. D. Holt, J. Menéndez, J. Simonis, and A. Schwenk, Three-nucleon forces and spectroscopy of neutron-rich calcium isotopes, Phys. Rev. C **90**, 024312 (2014).

[43] R. F. Garcia Ruiz, M. L. Bissell, K. Blaum, N. Frömmgen, M. Hammen, J. D. Holt, M. Kowalska, K. Kreim, J. Menéndez, R. Neugart, et al., Ground-state electromagnetic moments of calcium isotopes, Phys. Rev. C **91**, 041304 (2015).

Appendix: Experimental and theoretical results

Table II. Experimental and theoretical transition energies E_γ and transition strengths $B(M1)$, $B(E2)$ using FPD6, KB3G and GXPF1A interactions. For the two transitions where experimental E2/M1 multipole mixing ratios are available [21] the transitions strengths are marked with an $*$, while for the other mixed transitions upper limits of the transition strengths were calculated by assuming the extreme cases of pure M1 or E2 transition. The columns denoted by $B(\sigma L)^{\delta_{\rm SM}}_{\tau_{\rm exp}}$ contain transition strengths, calculated from the experimental lifetimes using mixing ratios deduced from the respective shell-model E2 and M1 strength and the corresponding $E_\gamma^{\rm exp}$.

Interaction	$J_i^\pi \to J_f^\pi$	$E_\gamma^{\rm exp}$ (keV)	$E_\gamma^{\rm SM}$ (keV)	$B(M1)_{\rm exp}$ (μ_N^2)	$B(E2)_{\rm exp}$ (e^2fm^4)	$B(M1)^{\delta_{\rm SM}}_{\tau_{\rm exp}}$ (μ_N^2)	$B(E2)^{\delta_{\rm SM}}_{\tau_{\rm exp}}$ (e^2fm^4)	$B(M1)_{\rm SM}$ (μ_N^2)	$B(E2)_{\rm SM}$ (e^2fm^4)	$\delta(E2/M1)$ SM + $E_\gamma^{\rm exp}$
FPD6	$5/2_1^- \to 3/2^-_{\rm g.s.}$	1237	611	≤ 0.04	≤ 370	$0.02^{+0.02}_{-0.01}$	$0.44^{+0.48}_{-0.17}$	0.02	0.46	0.05
	$5/2_2^- \to 3/2^-_{\rm g.s.}$		1352					0.12	104.1	
	$7/2^- \to 3/2^-_{\rm g.s.}$	1576	1471	–	63^{+40}_{-18}	–	–	–	62.4	-
	$7/2^- \to 5/2_1^-$	339	860	≤ 0.60	≤ 48000	$0.33^{+0.22}_{-0.10}$	3900^{+2600}_{-1200}	0.002	28.4	0.31
	$7/2^- \to 5/2_2^-$		120					0.17	29.2	
	$9/2^- \to 5/2_1^-$	968	1124	–	32^{+13}_{-9}	–	–	–	66.2	-
	$9/2^- \to 5/2_2^-$		383					–	38.4	-
	$9/2^- \to 7/2^-$	629	264	$0.07^{+0.03}_{-0.02}*$	$0.47^{+0.16}_{-0.10}*$	$0.07^{+0.03}_{-0.02}$	$13.1^{+4.4}_{-2.6}$	0.12	23.4	0.07
	$11/2^- \to 7/2^-$	921	1130	–	55^{+14}_{-11}	–	–	–	71.6	-
	$11/2^- \to 9/2^-$	292	866	$0.61^{+0.11}_{-0.08}*$	$280^{+230}_{-160}*$	$0.61^{+0.11}_{-0.08}$	$10.3^{+1.9}_{-1.4}$	0.11	0.95	0.01
	$13/2^- \to 11/2^-$	257	228	≤ 1.40	≤ 30000	$1.16^{+0.24}_{-0.17}$	$25.1^{+5.2}_{-3.7}$	0.42	20.4	0.01
KB3G	$5/2_1^- \to 3/2^-_{\rm g.s.}$	1237	1136	≤ 0.04	≤ 370	$0.02^{+0.02}_{-0.01}$	$4.4^{+4.8}_{-1.7}$	0.17	38.8	0.16
	$5/2_2^- \to 3/2^-_{\rm g.s.}$		1352					0.06	46.4	
	$7/2^- \to 3/2^-_{\rm g.s.}$	1576	1484	–	63^{+40}_{-18}	–	–	–	75.6	-
	$7/2^- \to 5/2_1^-$	339	348	≤ 0.60	≤ 48000	$0.36^{+0.24}_{-0.11}$	$4.5^{+2.9}_{-1.4}$	0.12	0.48	0.01
	$7/2^- \to 5/2_2^-$		132					0.17	2.35	
	$9/2^- \to 5/2_1^-$	968	987	–	32^{+13}_{-9}	–	–	–	93.3	-
	$9/2^- \to 5/2_2^-$		771					–	0.22	-
	$9/2^- \to 7/2^-$	629	639	$0.07^{+0.03}_{-0.02}*$	$0.47^{+0.16}_{-0.10}*$	$0.07^{+0.03}_{-0.02}$	$9.6^{+3.2}_{-1.9}$	0.12	14.9	0.06
	$11/2^- \to 7/2^-$	921	1095	–	55^{+14}_{-11}	–	–	–	57.8	-
	$11/2^- \to 9/2^-$	292	456	$0.61^{+0.11}_{-0.08}*$	$280^{+230}_{-160}*$	$0.61^{+0.11}_{-0.08}$	$10.3^{+1.9}_{-1.4}$	0.27	4.10	0.01
	$13/2^- \to 11/2^-$	257	251	≤ 1.40	≤ 30000	$1.16^{+0.24}_{-0.17}$	$25.1^{+5.2}_{-3.7}$	0.57	19.6	0.01
GXPF1A	$5/2_1^- \to 3/2^-_{\rm g.s.}$	1237	1356	≤ 0.04	≤ 370	$0.02^{+0.02}_{-0.01}$	$7.4^{+8.2}_{-2.8}$	0.20	81.4	0.21
	$5/2_2^- \to 3/2^-_{\rm g.s.}$		1742					0.002	11.0	
	$7/2^- \to 3/2^-_{\rm g.s.}$	1576	1413	–	63^{+40}_{-18}	–	–	–	75.8	-
	$7/2^- \to 5/2_1^-$	339	57	≤ 0.60	≤ 48000	$0.36^{+0.24}_{-0.11}$	$4.5^{+2.9}_{-1.4}$	0.26	0.94	0.01
	$9/2^- \to 5/2_1^-$	968	874	–	32^{+13}_{-9}	–	–	–	85.7	-
	$9/2^- \to 5/2_2^-$		488					–	0.02	-
	$9/2^- \to 7/2^-$	629	817	$0.07^{+0.03}_{-0.02}*$	$0.47^{+0.16}_{-0.10}*$	$0.07^{+0.03}_{-0.02}$	$13.1^{+4.4}_{-2.6}$	0.14	27.4	0.08
	$11/2^- \to 7/2^-$	921	975	–	55^{+14}_{-11}	–	–	–	69.3	-
	$11/2^- \to 9/2^-$	292	158	$0.61^{+0.11}_{-0.08}*$	$280^{+230}_{-160}*$	$0.61^{+0.11}_{-0.08}$	$10.3^{+1.9}_{-1.4}$	0.55	10.9	0.01
	$13/2^- \to 11/2^-$	257	389	≤ 1.40	≤ 30000	$1.16^{+0.24}_{-0.17}$	$100.4^{+20.9}_{-14.8}$	0.32	18.7	0.02